ELSEVIER

Journal of Alloys and Compounds 458 (2008) 166–173

Journal of ALLOYS AND COMPOUNDS

www.elsevier.com/locate/jallcom

Thermodynamic modeling of the Ce–Zn and Pr–Zn systems

C.P. Wang [a], X. Chen [a], X.J. Liu [a,*], F.S. Pan [b], K. Ishida [c]

[a] *Department of Materials Science and Engineering, College of Chemistry and Chemical Engineering, and Research Center of Materials Design and Applications, Xiamen University, Xiamen 361005, PR China*
[b] *College of Materials Science and Engineering, Chongqing University, Chongqing 400045, PR China*
[c] *Department of Materials Science, Graduate School of Engineering, Tohoku University, Sendai 980-8579, Japan*

Received 10 February 2007; received in revised form 23 March 2007; accepted 26 March 2007
Available online 30 March 2007

Abstract

In order to develop the thermodynamic database of phase equilibria in the Mg–Zn–Re (Re: rare earth element) base alloys, the thermodynamic assessments of the Ce–Zn and Pr–Zn systems were carried out by using the calculation of phase diagrams (CALPHAD) method on the basis of the experimental data including thermodynamic properties and phase equilibria. Based on the available experimental data, Gibbs free energies of the solution phases (liquid, bcc, fcc, hcp and dhcp) were modeled by the subregular solution model with the Redlich–Kister formula, and those of the intermetallic compounds were described by the sublattice model. A consistent set of thermodynamic parameters has been derived for describing the Gibbs free energies of each solution phase and intermetallic compound in the Ce–Zn and Pr–Zn binary systems. An agreement between the present calculated results and experimental data is obtained.

Keywords: Rare earth alloys and compounds; Phase diagrams; Thermodynamic modeling

1. Introduction

Magnesium (Mg) base alloys are potential candidates for structural, automotive and aerospace applications owing to their low density, high specific strength, high specific rigidity and good damping capacity. In particular, the Mg base alloys of the Mg–Zn series have great advantages for the development of low cost Mg base alloys due to high strength of considerable hardening response and good grain refinement by zirconium [1,2]. Rare earth elements are often added to Mg base alloys to improve their high temperature strength and creep resistance by precipitation hardness [3–5].

CALPHAD method is an important tool for designing new Mg base alloys because it can significantly decrease cost and time during development of materials and provides a clear guide line for material design [6]. In order to develop the thermodynamic database of phase equilibria in the Mg–Zn–Re base alloys, the thermodynamic description of each lower-order system which forms a part of this thermodynamic database is necessary. The purpose of this work is to present the thermodynamic descriptions of the Ce–Zn and the Pr–Zn binary systems by the CALPHAD method. The thermodynamic parameters of each phase in the Ce–Zn and Pr–Zn systems are optimized by fitting the experimental data on thermodynamic properties and phase equilibria.

2. Thermodynamic models

2.1. Solution phases

In the Ce–Zn and Pr–Zn systems, Gibbs free energies of the solution phases (liquid, fcc, bcc, hcp, dhcp) were described by the subregular solution model. The molar Gibbs free energy of each solution phase in these two systems is given as follows:

$$G_{\mathrm{m}}^{\phi} = \sum_{i=\mathrm{Re,Zn}} {}^{0}G_{i}^{\phi} x_i + RT \sum_{i=\mathrm{Re,Zn}} x_i \ln x_i + \Delta^{\mathrm{E}} G_{\mathrm{m}}^{\phi} \quad (1)$$

where ${}^{0}G_{i}^{\phi}$ denotes the Gibbs free energy of pure element in ϕ phase, which is taken from the SGTE pure element database [7]; Re means the element Ce or Pr; x_i represents the mole fraction of element i; R is the universal gas constant; T is the absolute tem-

* Corresponding author. Tel.: +86 592 2187888; fax: +86 592 2187966.
E-mail address: lxj@xmu.edu.cn (X.J. Liu).

0925-8388/$ – see front matter © 2007 Published by Elsevier B.V.
doi:10.1016/j.jallcom.2007.03.120

Table 1
The stable solid phases and the used models in the Ce–Zn system

Phase	Structure type	Modeling phase	Used models
γCe	Cu	fcc	Subregular solution model
δCe	W	bcc	Subregular solution model
(Zn)	Mg	hcp	Subregular solution model
CeZn	CsCl	(Ce)(Zn)	Sublattice model
$CeZn_2$	KHg_2	$(Ce)(Zn)_2$	Sublattice model
$CeZn_3$	$CEZn_3$	$(Ce)(Zn)_3$	Sublattice model
Ce_3Zn_{11}	La_3Al_{11}	$(Ce)_3(Zn)_{11}$	Sublattice model
$Ce_{13}Zn_{58}$	$Gd_{13}Zn_{58}$	$(Ce)_{13}(Zn)_{58}$	Sublattice model
$CeZn_5$	$CaCu_5$	$(Ce)(Zn)_5$	Sublattice model
Ce_3Zn_{22}	Ce_3Zn_{22}	$(Ce)_3(Zn)_{22}$	Sublattice model
αCe_2Zn_{17}	Th_2Ni_{17}	$(Ce)_2(Zn)_{17}$	Sublattice model
βCe_2Zn_{17}	Th_2Zn_{17}	$(Ce)_2(Zn)_{17}$	Sublattice model
$CeZn_{11}$	$BaCd_{11}$	$(Ce)(Zn)_{11}$	Sublattice model

perature; the term $\Delta^{E}G_{m}^{\phi}$ is the excess energy, which is expressed in the Redlich–Kister polynomials [8] as

$$\Delta^{E}G_{m}^{\phi} = x_{Re}x_{Zn}\sum_{i=0}^{n} {}^{i}L_{Re,Zn}^{\phi}(x_{Re} - x_{Zn})^{i} \quad (2)$$

where ${}^{i}L_{Re,Zn}^{\phi}$ is the binary interaction parameter, which is expressed as temperature dependence:

$${}^{i}L_{Re,Zn}^{\phi} = a + bT + cT\ln T \quad (3)$$

where the values of a, b and c are evaluated on the basis of the experimental data in the present work.

2.2. Stoichiometric intermetallic compounds

The intermetallic compounds of the CeZn, $CeZn_2$, $CeZn_3$, Ce_3Zn_{11}, $Ce_{13}Zn_{58}$, $CeZn_5$, Ce_3Zn_{22}, Ce_2Zn_{17} and $CeZn_{11}$ in the Ce–Zn binary system and PrZn, $\alpha PrZn_2$, $\beta PrZn_2$, $PrZn_3$, Pr_3Zn_{11}, $Pr_{13}Zn_{58}$, Pr_3Zn_{22}, αPr_2Zn_{17}, βPr_2Zn_{17} and $PrZn_{11}$ in the Pr–Zn binary system are treated as stoichiometric compounds. The Gibbs free energy per mole of formula unit Re_pZn_q is expressed as follows:

$$G_{m}^{Re_pZn_q} = \frac{p}{p+q}{}^{0}G_{Re}^{SER} + \frac{q}{p+q}{}^{0}G_{Zn}^{SER} + \Delta^{0}G_{f}^{Re_pZn_q} \quad (4)$$

Table 2
The stable solid phases and the used models in the Pr–Zn system

Phase	Structure type	Modeling phase	Used models
αPr	αLa	dhcp	Subregular solution model
βPr	W	bcc	Subregular solution model
(Zn)	Mg	hcp	Subregular solution model
PrZn	CsCl	(Pr)(Zn)	Sublattice model
$\alpha PrZn_2$	$CeCu_2$	$(Pr)(Zn)_2$	Sublattice model
$\beta PrZn_2$	–	$(Pr)(Zn)_2$	Sublattice model
$PrZn_3$	YZn_3	$(Pr)(Zn)_3$	Sublattice model
Pr_3Zn_{11}	Y_3Zn_{11}	$(Pr)_3(Zn)_{11}$	Sublattice model
$Pr_{13}Zn_{58}$	$Pu_{13}Zn_{58}$	$(Pr)_{13}(Zn)_{58}$	Sublattice model
Pr_3Zn_{22}	Pu_3Zn_{22}	$(Pr)_3(Zn)_{22}$	Sublattice model
αPr_2Zn_{17}	Th_2Ni_{17}	$(Pr)_2(Zn)_{17}$	Sublattice model
βPr_2Zn_{17}	Th_2Zn_{17}	$(Pr)_2(Zn)_{17}$	Sublattice model
$PrZn_{11}$	$BaCd_{11}$	$(Pr)(Zn)_{11}$	Sublattice model

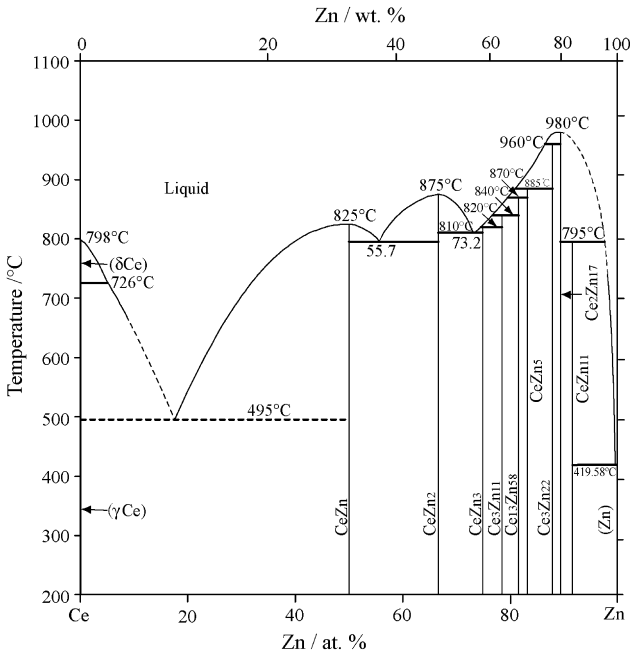

Fig. 1. The phase diagram of the Ce–Zn system reviewed by Okamoto [12].

where $\Delta^{0}G_{f}^{Re_pZn_q}$ represents the Gibbs free energy of formation per mole of formula unit Re_pZn_q referred to the standard element reference (SER) state of the component elements, which is described as

$$\Delta^{0}G_{f}^{Re_pZn_q} = a' + b'T \quad (5)$$

where the values of a' and b' are evaluated in the present work.

The stable solid phases and the used models in the Ce–Zn and Pr–Zn systems are listed in Tables 1 and 2, respectively.

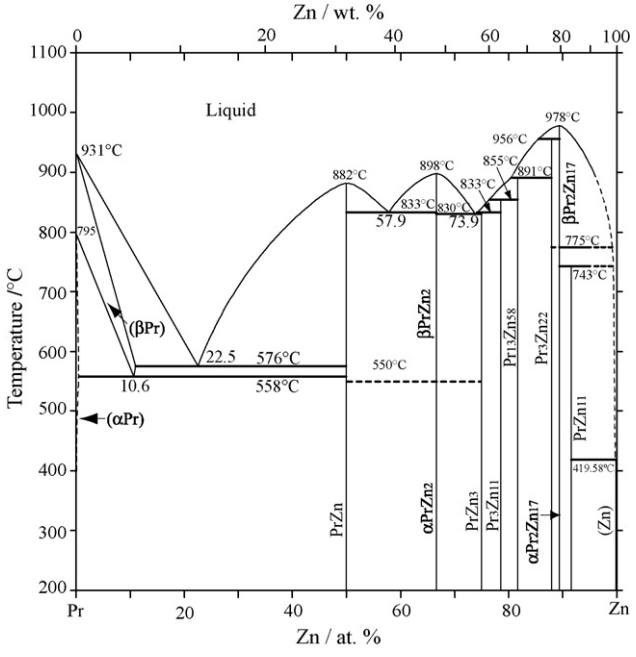

Fig. 2. The phase diagram of the Pr–Zn system reviewed by Okamoto [12].

Table 3
Thermodynamic parameters in the Ce–Zn system

Parameters in each phase (J/mol)
Liquid phase, format (Ce, Zn)
${}^0L^{\mathrm{Liq}}_{\mathrm{Ce,Zn}} = -116372.167 + 39.3T$
${}^1L^{\mathrm{Liq}}_{\mathrm{Ce,Zn}} = 70000 - 19T$
${}^2L^{\mathrm{Liq}}_{\mathrm{Ce,Zn}} = -42000 + 20T$
Fcc phase, format (Ce, Zn)
${}^0L^{\mathrm{Fcc}}_{\mathrm{Ce,Zn}} = -2000$
CeZn compound, format $(Ce)_{0.5}(Zn)_{0.5}$
${}^0G^{\mathrm{CeZn}}_{\mathrm{Ce:Zn}} - 0.5{}^0G^{\mathrm{fcc}}_{\mathrm{Ce}} - 0.5{}^0G^{\mathrm{hcp}}_{\mathrm{Zn}} = -34040 + 6.4T$
$CeZn_2$ compound, format $(Ce)_{0.333}(Zn)_{0.667}$
${}^0G^{\mathrm{CeZn_2}}_{\mathrm{Ce:Zn}} - 0.333{}^0G^{\mathrm{fcc}}_{\mathrm{Ce}} - 0.667{}^0G^{\mathrm{hcp}}_{\mathrm{Zn}} = -40060 + 9.22T$
$CeZn_3$ compound, format $(Ce)_{0.25}(Zn)_{0.75}$
${}^0G^{\mathrm{CeZn_3}}_{\mathrm{Ce:Zn}} - 0.25{}^0G^{\mathrm{fcc}}_{\mathrm{Ce}} - 0.75{}^0G^{\mathrm{hcp}}_{\mathrm{Zn}} = -38473.75 + 9.83T$
Ce_3Zn_{11} compound, format $(Ce)_{0.214}(Zn)_{0.786}$
${}^0G^{\mathrm{Ce_3Zn_{11}}}_{\mathrm{Ce:Zn}} - 0.214{}^0G^{\mathrm{fcc}}_{\mathrm{Ce}} - 0.786{}^0G^{\mathrm{hcp}}_{\mathrm{Zn}} = -36882.7 + 9.286T$
$Ce_{13}Zn_{58}$ compound, format $(Ce)_{0.183}(Zn)_{0.817}$
${}^0G^{\mathrm{Ce_{13}Zn_{58}}}_{\mathrm{Ce:Zn}} - 0.183{}^0G^{\mathrm{fcc}}_{\mathrm{Ce}} - 0.817{}^0G^{\mathrm{hcp}}_{\mathrm{Zn}} = -35352.77 + 8.94T$
$CeZn_5$ compound, format $(Ce)_{0.167}(Zn)_{0.833}$
${}^0G^{\mathrm{CeZn_5}}_{\mathrm{Ce:Zn}} - 0.167{}^0G^{\mathrm{fcc}}_{\mathrm{Ce}} - 0.833{}^0G^{\mathrm{hcp}}_{\mathrm{Zn}} = -34491.67 + 8.883T$
Ce_3Zn_{22} compound, format $(Ce)_{0.12}(Zn)_{0.88}$
${}^0G^{\mathrm{Ce_3Zn_{22}}}_{\mathrm{Ce:Zn}} - 0.12{}^0G^{\mathrm{fcc}}_{\mathrm{Ce}} - 0.88{}^0G^{\mathrm{hcp}}_{\mathrm{Zn}} = -30196 + 7.4T$
Ce_2Zn_{17} compound, format $(Ce)_{0.105}(Zn)_{0.895}$
${}^0G^{\mathrm{Ce_2Zn_{17}}}_{\mathrm{Ce:Zn}} - 0.105{}^0G^{\mathrm{fcc}}_{\mathrm{Ce}} - 0.895{}^0G^{\mathrm{hcp}}_{\mathrm{Zn}} = -27973.68 + 6.526T$
$CeZn_{11}$ compound, format $(Ce)_{0.083}(Zn)_{0.917}$
${}^0G^{\mathrm{CeZn_{11}}}_{\mathrm{Ce:Zn}} - 0.083{}^0G^{\mathrm{fcc}}_{\mathrm{Ce}} - 0.917{}^0G^{\mathrm{hcp}}_{\mathrm{Zn}} = -24495.83 + 6.5T$

Table 4
Thermodynamic parameters in the Pr–Zn system

Parameters in each phase (J/mol)
Liquid phase, format (Pr, Zn)
${}^0L^{\mathrm{Liq}}_{\mathrm{Pr,Zn}} = -112893.879 + 28.008T$
${}^1L^{\mathrm{Liq}}_{\mathrm{Pr,Zn}} = 73587.04 - 21.204T$
${}^2L^{\mathrm{Liq}}_{\mathrm{Pr,Zn}} = -34066.071 + 10.39T$
dhcp phase, format (Pr, Zn)
${}^0G^{\mathrm{dhcp}}_{\mathrm{Zn}} - {}^0G^{\mathrm{hcp}}_{\mathrm{Zn}} = 2108.72$
${}^0L^{\mathrm{dhcp}}_{\mathrm{Pr,Zn}} = -39139.65 + 5.422T$
bcc phase, format (Pr, Zn)
${}^0L^{\mathrm{bcc}}_{\mathrm{Pr,Zn}} = -67287.643 - 35.723T + 4.138T\ln T$
${}^1L^{\mathrm{bcc}}_{\mathrm{Pr,Zn}} = 27339.80$
PrZn compound, format $(Pr)_{0.5}(Zn)_{0.5}$
${}^0G^{\mathrm{PrZn}}_{\mathrm{Pr:Zn}} - 0.5{}^0G^{\mathrm{dhcp}}_{\mathrm{Pr}} - 0.5{}^0G^{\mathrm{hcp}}_{\mathrm{Zn}} = -32430 + 2.725T$
$\alpha PrZn_2$ compound, format $(Pr)_{0.333}(Zn)_{0.667}$
${}^0G^{\mathrm{\alpha PrZn2}}_{\mathrm{Pr:Zn}} - 0.333{}^0G^{\mathrm{dhcp}}_{\mathrm{Pr}} - 0.667{}^0G^{\mathrm{hcp}}_{\mathrm{Zn}} = -35866.67 + 3.73T$
$\beta PrZn_2$ compound, format $(Pr)_{0.333}(Zn)_{0.667}$
${}^0G^{\mathrm{\beta PrZn_2}}_{\mathrm{Pr:Zn}} - 0.333{}^0G^{\mathrm{dhcp}}_{\mathrm{Pr}} - 0.667{}^0G^{\mathrm{hcp}}_{\mathrm{Zn}} = -35619.68 + 3.43T$
$PrZn_3$ compound, format $(Pr)_{0.25}(Zn)_{0.75}$
${}^0G^{\mathrm{PrZn_3}}_{\mathrm{Pr:Zn}} - 0.25{}^0G^{\mathrm{dhcp}}_{\mathrm{Pr}} - 0.75{}^0G^{\mathrm{hcp}}_{\mathrm{Zn}} = -34917.5 + 4.88T$
Pr_3Zn_{11} compound, format $(Pr)_{0.214}(Zn)_{0.786}$
${}^0G^{\mathrm{Pr_3Zn_{11}}}_{\mathrm{Pr:Zn}} - 0.214{}^0G^{\mathrm{dhcp}}_{\mathrm{Pr}} - 0.786{}^0G^{\mathrm{hcp}}_{\mathrm{Zn}} = -34120.71 + 5.22T$
$Pr_{13}Zn_{58}$ compound, format $(Pr)_{0.183}(Zn)_{0.817}$
${}^0G^{\mathrm{Pr_{13}Zn_{58}}}_{\mathrm{Pr:Zn}} - 0.183{}^0G^{\mathrm{dhcp}}_{\mathrm{Pr}} - 0.817{}^0G^{\mathrm{hcp}}_{\mathrm{Zn}} = -33303.94 + 5.671T$
Pr_3Zn_{22} compound, format $(Pr)_{0.12}(Zn)_{0.88}$
${}^0G^{\mathrm{Pr_3Zn_{22}}}_{\mathrm{Pr:Zn}} - 0.12{}^0G^{\mathrm{dhcp}}_{\mathrm{Pr}} - 0.88{}^0G^{\mathrm{hcp}}_{\mathrm{Zn}} = -30350 + 6.488T$
αPr_2Zn_{17} compound, format $(Pr)_{0.105}(Zn)_{0.895}$
${}^0G^{\mathrm{\alpha Pr_2Zn_{17}}}_{\mathrm{Pr:Zn}} - 0.105{}^0G^{\mathrm{dhcp}}_{\mathrm{Pr}} - 0.895{}^0G^{\mathrm{hcp}}_{\mathrm{Zn}} = -29228.63 + 6.632T$
βPr_2Zn_{17} compound, format $(Pr)_{0.105}(Zn)_{0.895}$
${}^0G^{\mathrm{\beta Pr_2Zn_{17}}}_{\mathrm{Pr:Zn}} - 0.105{}^0G^{\mathrm{dhcp}}_{\mathrm{Pr}} - 0.895{}^0G^{\mathrm{hcp}}_{\mathrm{Zn}} = -28897.66 + 6.316T$
$PrZn_{11}$ compound, format $(Pr)_{0.083}(Zn)_{0.917}$
${}^0G^{\mathrm{PrZn_{11}}}_{\mathrm{Pr:Zn}} - 0.083{}^0G^{\mathrm{dhcp}}_{\mathrm{Pr}} - 0.917{}^0G^{\mathrm{hcp}}_{\mathrm{Zn}} = -24687.5 + 6.025T$

3. Experimental information

3.1. Ce–Zn system

The phase diagram in the Ce–Zn system was mainly investigated by Chiotti and Mason [9], who measured the whole composition range of the phase diagram by differential thermal analysis (DTA), metallography and X-ray diffraction, and determined the phase stability of the CeZn, $CeZn_2$, $CeZn_3$, $CeZn_{3.67}$, $CeZn_{4.5}$, $CeZn_{5.25}$, $CeZn_7$, $CeZn_{8.5}$ and $CeZn_{11}$ compounds. Based on the vapor-pressure data obtained by the dewpoint method, the equations for the excess molar Gibbs free energy of liquid alloys and the Gibbs free energies, enthalpies and entropies of formation for the intermetallic compounds were also derived by Chiotti and Mason [9]. Johnson and Yonco [10] measured the electromotive force between pure Ce and an alloy consisting of zinc-rich liquid in equilibrium with $CeZn_{11}$ by using a fused-salt cell method and gave the equations for the standard Gibbs free energy of formation of the $CeZn_{11}$ phase. Later, Johnson and Yonco [11] studied the Ce–Zn system by using a high-temperature galvanic cell method and obtained a similar equation for the standard Gibbs free energy of formation of the $CeZn_{11}$ phase and an equation for the partial molar excess Gibbs free energy of Ce in dilute solutions of Ce in liquid Zn.

Okamoto [12] reviewed the phase diagram of the Ce–Zn system, based on the experimental data [9], with slight changes in compositions of some compounds ($Ce_{13}Zn_{58}$ for $CeZn_{4.5}$ [13], $CeZn_5$ for $CeZn_{5.25}$ [14], and Ce_3Zn_{22} for $CeZn_7$ [15]), as shown in Fig. 1, where the liquidus temperature in the Zn-rich portion is still being tentative. According to the experimental results of Chiotti and Mason [9], the possibility of a eutectoid reaction at about 500 °C was suggested by thermal-analyses data, however, which was not confirmed by either metallographic or X-ray data.

3.2. Pr–Zn system

The phase diagram in the Pr–Zn system was mainly investigated by Mason and Chiotti [16], who measured the whole composition range of the phase diagram by using the metallographic, thermal, X-ray and resistivity data, and determined the phase stability of the PrZn, $PrZn_2$, $PrZn_3$, Pr_3Zn_{11}, $Pr_{13}Zn_{58}$, Pr_3Zn_{22}, Pr_2Zn_{17} and $PrZn_{11}$ compounds. Saccone et al. [17] studied the Pr–Zn phase diagram in the Pr-rich region up to 50 at.% Zn and confirmed the literature data from Mason and Chiotti [16], with slight differences in the temperature of the invariant equilibria by differential thermal analysis, X-ray powder diffractometry, metallographic analysis and quantitative electron probe microanalysis.

Table 5
Experimental and calculated invariant reactions in the Ce–Zn system

Invariant reaction	Reaction type		Composition at.% Zn		Temperature °C	Reference
$L \leftrightarrow \gamma Ce + CeZn$	Eutectic	~17.6	–	50.0	~495	[9]
		18.3	0.1	50.0	499	This work
$L \leftrightarrow CeZn + CeZn_2$	Eutectic	55.7	50.0	66.7	795	[9]
		56.5	50.0	66.7	794	This work
$L \leftrightarrow CeZn_2 + CeZn_3$	Eutectic	73.2	66.7	75.0	810	[9]
		73.7	66.7	75.0	817	This work
$L + Ce_3Zn_{11} \leftrightarrow CeZn_3$	Peritectic	74.3	78.6	75.0	820	[9]
		74.0	78.6	75.0	817	This work
$L + Ce_{13}Zn_{58} \leftrightarrow Ce_3Zn_{11}$	Peritectic	76.5	81.7	78.6	840	[9]
		76.5	81.7	78.6	839	This work
$L + CeZn_5 \leftrightarrow Ce_{13}Zn_{58}$	Peritectic	79.6	83.3	81.7	870	[9]
		79.4	83.3	81.7	870	This work
$L + Ce_3Zn_{22} \leftrightarrow CeZn_5$	Peritectic	81.0	88.0	83.3	885	[9]
		81.1	88.0	83.3	886	This work
$L + Ce_2Zn_{17} \leftrightarrow Ce_3Zn_{22}$	Peritectic	86.6	89.5	88.0	960	[9]
		86.2	89.5	88.0	959	This work
$L + Ce_2Zn_{17} \leftrightarrow CeZn_{11}$	Peritectic	97.8	89.5	91.7	795	[9]
		97.5	89.5	91.7	795	This work
$L \leftrightarrow CeZn$	Congruent		–		825	[9]
					825	This work
$L \leftrightarrow CeZn_2$	Congruent		–		875	[9]
					875	This work
$L \leftrightarrow Ce_2Zn_{17}$	Congruent		–		980	[9]
					980	This work

However, the congruent melting temperature of the PrZn phase determined by Saccone et al. [17] is 900 °C, and the corresponding result from Mason and Chiotti [16] is 882 °C.

Chiotti and Mason [18] derived the equations for the excess molar Gibbs free energy of liquid alloys and the Gibbs free energies, enthalpies and entropies of formation for the intermetallic compounds based on the vapor-pressure data obtained by the dewpoint method, Johnson and Yonco [11] also obtained the equations for the standard Gibbs free energy of formation of the $PrZn_{11}$ phase and the partial molar excess Gibbs free energy of Pr in dilute solutions of Pr in liquid Zn by means of the electromotive force measurements.

Okamoto [12] reviewed the phase diagram of the Pr–Zn system, based on the experimental data [16], as shown in Fig. 2, in which the temperature of the polymorphic transformation in $PrZn_2$ and the liquidus temperature in the Zn-rich portion are still being tentative.

4. Optimized results and discussion

The optimization of the thermodynamic parameters of the various phases was performed with PARROT module of the

Table 6
Gibbs free energies of formation of intermetallic compounds in the Ce–Zn system

Phase	Gibbs free energy of formation (kJ/mol of atoms)					
	500 °C		700 °C		900 °C	
	Present calculation	Experimental data [9,11]	Present calculation	Experimental data [9,11]	Present calculation	Experimental data [9,11]
CeZn	−28.67	−29.75	−26.31	−26.81	−23.96	−23.88
$CeZn_2$	−32.36	−33.13	−29.09	−29.57	−25.82	−25.87
$CeZn_3$	−30.23	−31.05	−26.66	−27.46	−23.08	−23.67
Ce_3Zn_{11}	−29.03	−29.91	−25.49	−26.27	−21.95	−22.38
$Ce_{13}Zn_{58}$	−27.74	−28.70	−24.20	−25.02	−20.66	−21.05
$CeZn_5$	−26.91	−27.61	−23.35	−23.88	−19.79	−19.85
Ce_3Zn_{22}	−23.72	−25.33	−20.36	−21.61	−16.99	−17.56
Ce_2Zn_{17}	−22.16	−23.55	−18.94	−19.88	−15.72	−15.87
$CeZn_{11}$	−18.69	−19.60	−15.42	−16.02	−12.16	−12.06
		−18.53*		−15.39*		−12.25*

The reference states of pure elements of Ce and Zn are fcc and liquid phases, respectively. *Note*: Results with "*" are from Ref. [11], the others are from Ref. [9].

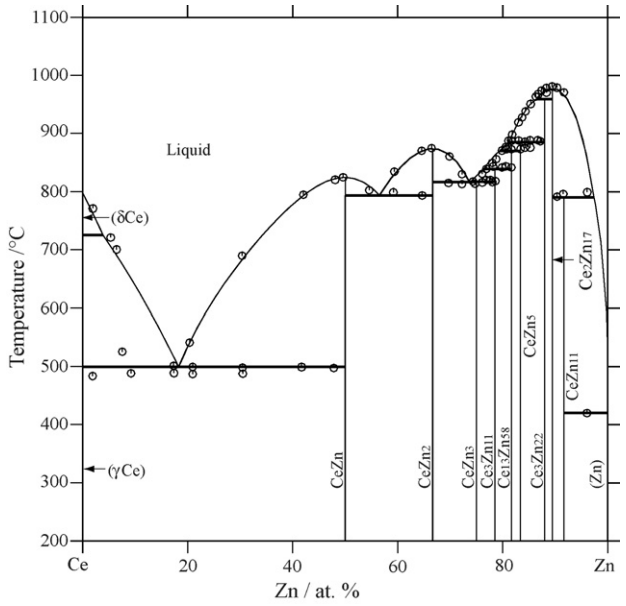

Fig. 3. The calculated phase diagram of the Ce–Zn system with experimental data [9].

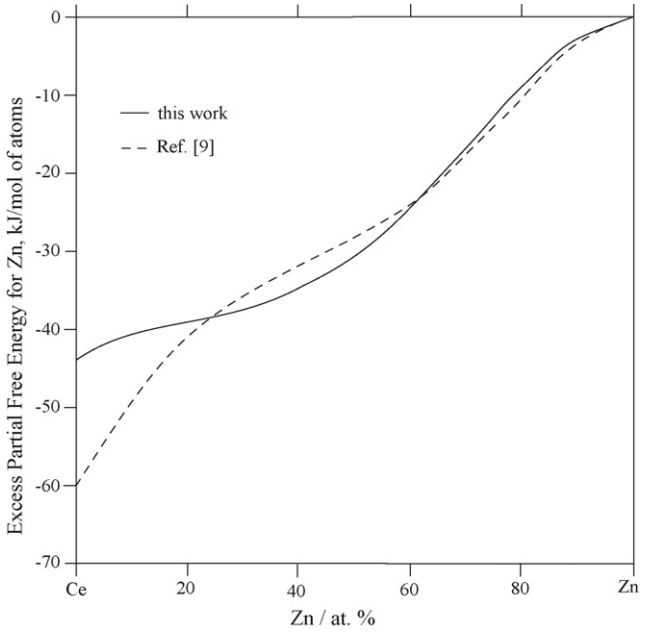

Fig. 5. The calculated excess partial molar Gibbs free energy for Zn of liquid alloys at 827 °C (1100 K) in the Ce–Zn system with experimental data [9].

Thermo-Calc package, which takes various types of experimental data for the optimization process [19]. The experimental data of the phase diagram and thermodynamic properties were used as input to the program. Each piece of selected information was offered a certain weight according to the importance of the data, which was changed by trial and error during the assessment, until most of them is reproduced within the expected uncertainty limits.

All the parameters were eventually optimized to obtain the best consistency between calculated results and experimental data. All evaluated parameters in the Ce–Zn and Pr–Zn systems are listed in the Tables 3 and 4, respectively.

4.1. Ce–Zn system

For the Ce–Zn binary system, the experimental data on phase diagram and thermodynamic properties [9,11] were used in the optimization. It is noted that the Ce_2Zn_{17} compound has two types of structure according to the experimental results of Iandelli and Palenzone [20]. But the Ce_2Zn_{17} compound is modeled as one phase in this study

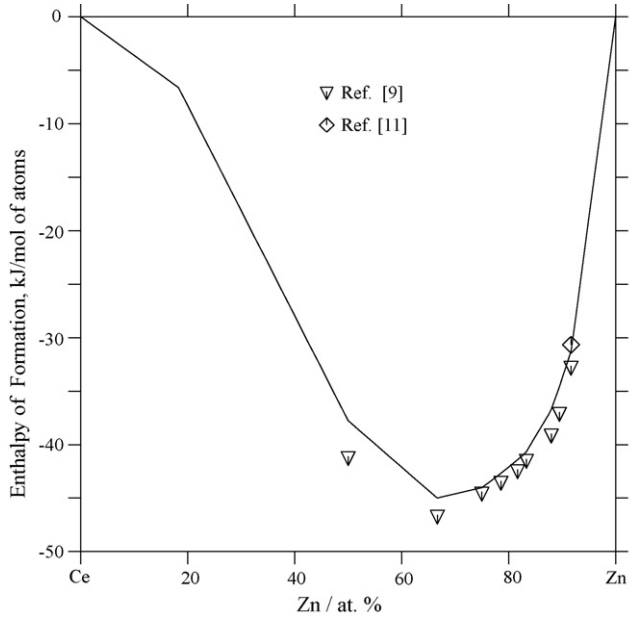

Fig. 4. The calculated enthalpies of formation of intermetallic compounds in the Ce–Zn system at 500 °C compared with experimental data [9,11]. The reference states of pure elements of Ce and Zn are fcc and liquid phases, respectively.

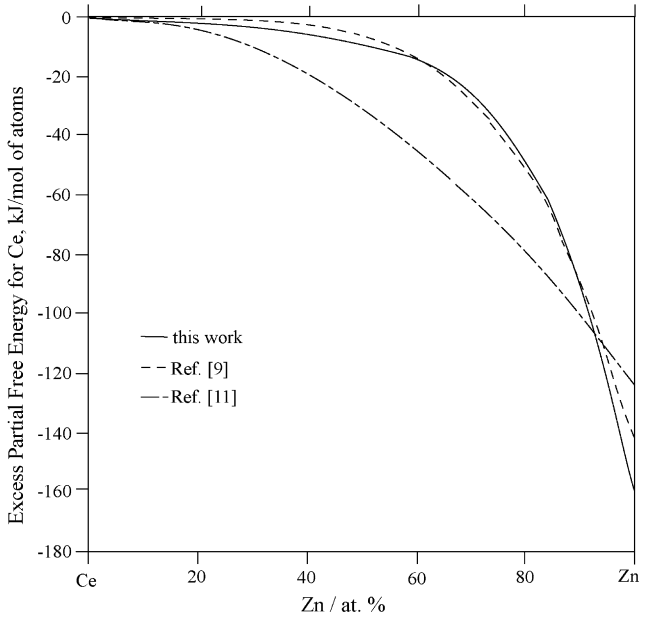

Fig. 6. The calculated excess partial molar Gibbs free energy for Ce of liquid alloys at 827 °C (1100 K) in the Ce–Zn system with experimental data [9,11].

Table 7
Experimental and calculated invariant reactions in the Pr–Zn system

Invariant reaction	Reaction type	Composition at.% Zn			Temperature °C	Reference
L ↔ bcc_A2 + PrZn	Eutectic	22.5	–	50.0	576	[16]
		21.5	14	50.0	570	[17]
		21.7	12.5	50.0	572	This work
L ↔ PrZn + βPrZn$_2$	Eutectic	57.9	50.0	66.7	833	[16]
		58.4	50.0	66.7	822	This work
L ↔ βPrZn$_2$ + PrZn$_3$	Eutectic	73.9	66.7	75.0	830	[16]
		73.2	66.7	75.0	830	This work
L + Pr$_3$Zn$_{11}$ ↔ PrZn$_3$	Peritectic	74.4	78.6	75.0	833	[16]
		74.6	78.6	75.0	834	This work
L + Pr$_{13}$Zn$_{58}$ ↔ Pr$_3$Zn$_{11}$	Peritectic	76.6	81.7	78.6	855	[16]
		77.1	81.7	78.6	856	This work
L + Pr$_3$Zn$_{22}$ ↔ Pr$_{13}$Zn$_{58}$	Peritectic	80.0	88.0	81.7	891	[16]
		81.5	88.0	81.7	891	This work
L + βPr$_2$Zn$_{17}$ ↔ Pr$_3$Zn$_{22}$	Peritectic	85.6	89.5	88.0	956	[16]
		86.0	89.5	88.0	956	This work
L + Pr$_2$Zn$_{17}$ ↔ PrZn$_{11}$	Peritectic	89.5	89.5	91.7	743	[16]
		89.5	89.5	91.7	743	This work
dhcp + PrZn ↔ bcc_A2	Eutectoid	–	50.0	10.6	558	[16]
		2	50.0	11	550	[17]
		1.5	50.0	11.5	550	This work
βPrZn$_2$ ↔ αPrZn$_2$	Polymorphic-transformation				~550	[16]
			–		550	This work
βPr$_2$Zn$_{17}$ ↔ αPr$_2$Zn$_{17}$	Polymorphic-transformation				775	[11]
			–		775	This work
L ↔ PrZn	Congruent		–		882	[11]
					900	[19]
					884	This work
L ↔ PrZn$_2$	Congruent		–		898	[11]
					898	This work
L ↔ Pr$_2$Zn$_{17}$	Congruent		–		978	[11]
					978	This work

Table 8
Gibbs free energies of formation of intermetallic compounds at 500 °C in the Pr–Zn system

Phase	Gibbs free energy of formation (kJ/mol of atoms)	
	Present calculation	Experimental data [11,18]
PrZn	−29.90	−29.88
αPrZn$_2$	−32.41	−32.54
βPrZn$_2$	–	–
PrZn$_3$	−30.50	−30.40
Pr$_3$Zn$_{11}$	−29.41	−29.33
Pr$_{13}$Zn$_{58}$	−28.22	−28.15
Pr$_3$Zn$_{22}$	−24.58	−24.28
αPr$_2$Zn$_{17}$	−23.34	−22.92
βPr$_2$Zn$_{17}$	–	–
PrZn$_{11}$	−19.25	−18.91
		−18.25*

The reference states of pure elements of Pr and Zn are dhcp and liquid phases, respectively. *Note*: Results with "*" are from Ref. [11], the others are from Ref. [18].

because the relative polymorphic transformation data are meager.

The calculated Ce–Zn phase diagram is shown in Fig. 3 together with the experimental data. All the invariant reactions in the Ce–Zn system with experimental data [9] are listed in Table 5. The calculated phase diagram is in excellent agreement with the experimental results reported by Chiotti and Mason [9].

The calculated values of the Gibbs free energies of formation of all stoichiometric compounds in the Ce–Zn system at 500, 700 and 900 °C together with experimental data [9,11] are listed in Table 6. The calculated enthalpies of formation of the intermetallic phases at 500 °C with experimental data [9,11] are shown in Fig. 4, where the reference states of pure elements of Ce and Zn are the fcc and liquid phases, respectively. Fig. 5 shows the excess partial molar Gibbs free energy for Zn of liquid alloys at 827 °C (1100 K) with experimental data [9]. It is seen that there is a discrepancy between our calculated results at the Ce-rich side and the calculated results given by Chiotti and Mason [9], as shown in Fig. 5. Since Chiotti and Mason [9] gave

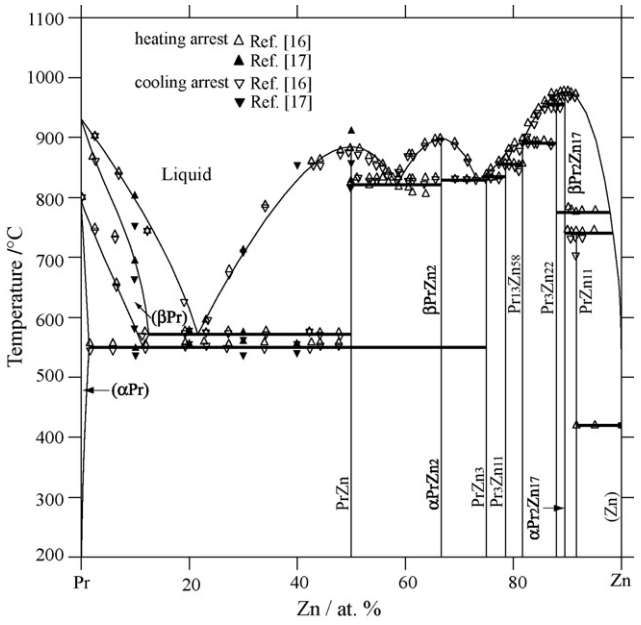

Fig. 7. The calculated phase diagram of the Pr–Zn system with experimental data [16,17].

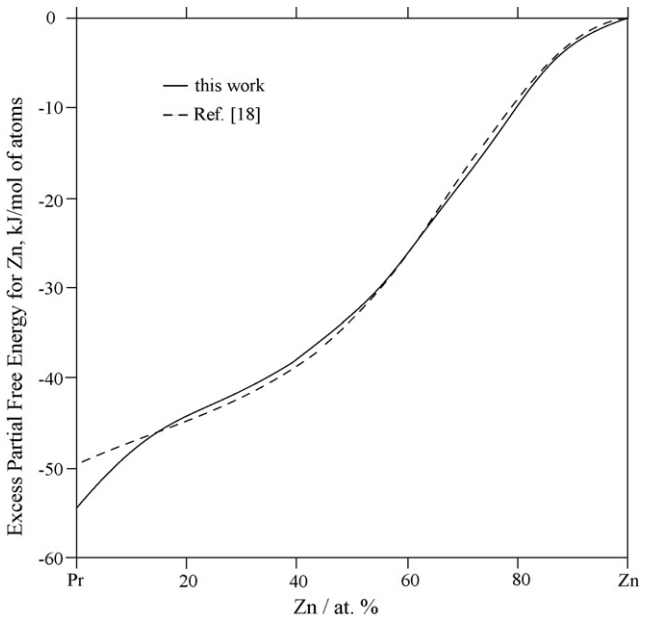

Fig. 9. The calculated excess partial molar Gibbs free energy for Zn of liquid alloys at 827 °C (1100 K) in the Pr–Zn system with experimental data [18].

the composition dependence of the equation in the range from 0 to 17.7 at.% Zn by extrapolation, thus our calculated results are considered to be acceptable. Fig. 6 shows the excess partial molar Gibbs free energy for Ce of liquid alloys at 827 °C (1100 K) with experimental data [9,11].

4.2. Pr–Zn system

For the Pr–Zn binary system, the experimental data on the phase diagram and thermodynamic properties [11,16–18] were used in the optimization. The calculated Pr–Zn phase diagram together with the experimental data is shown in Fig. 7. All the invariant reactions in the Pr–Zn system compared with experimental data [16] are listed in Table 7. The calculated phase diagram is in excellent agreement with most of the experimental results reported by Mason and Chiotti [16].

The calculated and experimental values [11,18] of the Gibbs free energies of all stoichiometric compounds in the Pr–Zn system at 500 °C are listed in Table 8. And the calculated enthalpies of formation of the intermetallic phases at 500 °C with experimental data [11,18] are shown in Fig. 8, where the reference

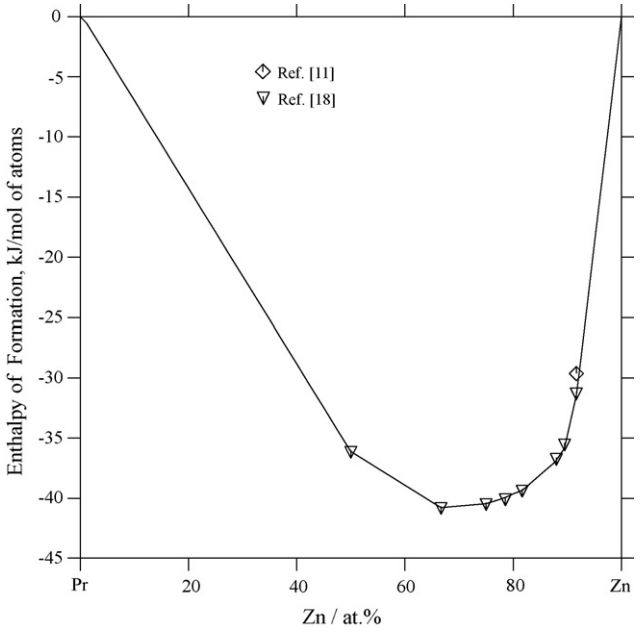

Fig. 8. The calculated enthalpies of formation of intermetallic compounds in the Pr–Zn system at 500 °C compared with experimental data [11,18]. The reference states of pure elements of Pr and Zn are dhcp and liquid phases, respectively.

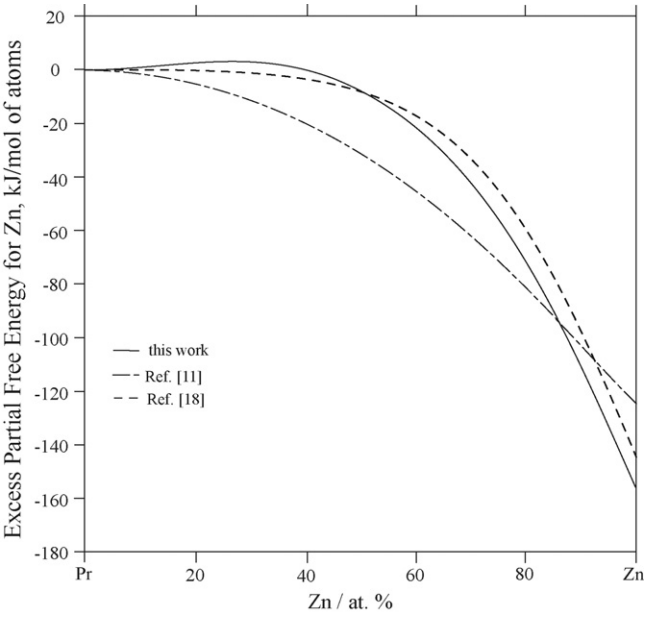

Fig. 10. The calculated excess partial molar Gibbs free energy for Pr of liquid alloys at 827 °C (1100 K) in the Pr–Zn system with experimental data [11,18].

states of pure elements of Pr and Zn are dhcp and liquid phases, respectively. Figs. 9 and 10 show the excess partial molar Gibbs free energies for Zn and Pr of liquid alloys at 827 °C 100 K) with experimental data [11,18]. A good agreement is obtained between the present calculated results and experimental data.

5. Conclusions

The phase diagrams and thermodynamic properties in the Ce–Zn and Pr–Zn binary systems were evaluated by combining the thermodynamic models with the available experimental information in literature. A consistent set of optimized thermodynamic parameters has been derived for describing the Gibbs free energy of each solution phase and intermetallic compound in the Ce–Zn and Pr–Zn binary system, and good agreement between the calculated results and most of the experimental data is obtained.

Acknowledgements

This work was jointly supported by the National Outstanding Youth Science Foundation of China (No. 50425101), the Ministry of Science and Technology, PR China (No. 2004CCA04200) and the Ministry of Education, PR China (Nos. 20050384003 and 105100), Fujian Natural Science Foundation (E0310023), and Chongqing Science and Technology Commission. And the Support from a Grant-in-Aid Core Research for Evolutional Science, and Technology (CREST), Japan Science and Technology Agency (JST) is also acknowledged.

References

[1] I.J. Polmear, Light Alloys, 3rd ed., Arnold, London, 1995.
[2] M.M. Avedesian, H. Baker (Eds.), Magnesium and Magnesium Alloys, ASM, USA, 1999.
[3] B.L. Mordike, T. Ebert, Mater. Sci. Eng. A 302 (2001) 37–45.
[4] N. Al-Aqeeli, G. Mendoza-Suarez, A. Labrie, R.A.L. Drew, J. Alloys Compd. 400 (2005) 96–99.
[5] I.P. Moreno, T.K. Nandy, J.W. Jones, J.E. Allison, T.M. Pollock, Scripta Mater. 48 (2003) 1029–1034.
[6] L. Kaufman, H. Bernstein, Computer Calculation of Phase Diagram, Academic Press, New York, 1970.
[7] A.T. Dinsdale, CALPHAD 15 (1991) 317–425.
[8] O. Redlich, A.T. Kister, Ind. Eng. Chem. 40 (1948) 345–348.
[9] P. Chiotti, J.T. Mason, Trans. Metall. Soc. AIME 233 (4) (1965) 786–795.
[10] I. Johnson, R.M. Yonco, U.S. Atomic Energy Commission Research and Development Report ANL 6231, Office of Technical Services, U.S. Department of Commerce, Washington 25, DC, 1960, p. 78.
[11] I. Johnson, R.M. Yonco, Met. Trans. 1 (4) (1970) 905–910.
[12] H. Okamoto, Desk Handbook—Phase Diagrams for Binary Alloys, ASM International, 2000.
[13] G. Bruzzone, M.L. Fornasini, F. Merlo, J. Less-Common Met. 22 (3) (1970) 253–264.
[14] E. Veleckis, C.L. Rosen, H.M. Feder, J. Phys. Chem. 65 (2) (1961) 127–2131.
[15] P.I. Kripyakevich, Yu.B. Kuz'ma, N.S. Ugrin, Zh. Struk. Khim. 8 (4) (1967) 703–705 (in Russian);
P.I. Kripyakevich, Yu.B. Kuz'ma, N.S. Ugrin, TR: J. Struct. Chem. 8 (4) (1967) 632–633.
[16] J.T. Mason, P. Chiotti, Met. Trans. 1 (8) (1970) 2119–2123.
[17] A. Saccone, A.M. Cardinale, S. Delfino, G. Cacciamani, R. Ferro, J. Alloys Compd. 317/318 (2001) 503–512.
[18] P. Chiotti, J.T. Mason, Met. Trans. 2 (4) (1971) 967–973.
[19] B. Sundman, B. Jansson, J.-O. Anderson, CALPHAD 9 (1985) 153–190.
[20] A. Iandelli, A. Palenzone, J. Less-Common Met. 12 (3) (1967) 333–343.